

A vulnerability assessment method to evaluate the impact of tunnel drainage on terrestrial vegetation under various atmospheric and climatic conditions



Cagri Gokdemir^a, Yoram Rubin^b, Xiaojun Li^{a,*}, Hao Xu^a

^a Department of Geotechnical Engineering, College of Civil Engineering, Tongji University, 1239 Siping Road, Shanghai 200092, China

^b Department of Civil and Environmental Engineering, University of California, Berkeley, CA 94720-1716, USA

ARTICLE INFO

Keywords:

Soil-plant-atmosphere continuum
Root zone wilting
Soil water budget
Soil water pressure
Tunnel drainage
Environmental vulnerability assessment

ABSTRACT

The impact of tunnel drainage on local water resources has attracted increasing attention in the past decades. The potential impacts of tunnel drainage on terrestrial vegetation have been evaluated from a groundwater environment perspective. However, previous attempts did not consider the atmospheric and climatic conditions along with the change to the regional groundwater table. To address the lack of atmospheric influence, this study proposes a vulnerability assessment method focused on the soil-plant-atmosphere continuum by taking tunnel drainage, atmospheric and climatic impacts into account. The proposed method consists of five stages: (1) groundwater seepage model for water table distribution, (2) topsoil model based on a single column perspective for soil water pressure distributions, (3) dynamic root-zone wilting for the transient model, (4) Budyko-type analysis for the soil water storage under longer-term climatic changes, and (5) summary based on the outcomes of vulnerability analysis. The case study was located in the Yuexi county (Anhui, East China) and was investigated based on different soil textures, weather conditions, and groundwater table drawdown scenarios. Transient intra-annual water pressure dynamics were simulated for one year, and aggregate variations of soil water storage were summarized using the Budyko framework. The assessment method demonstrated that the textural differences and climatic changes are more impactful on plant vulnerability compared to the drainage effect in the specific case. The increase in aridity towards the sub-humid dry climate drives the soil columns to decrease the water storage, where the significant loss of water storage was also observed in the Budyko-type framework. The outcomes suggest that under sub-humid dry conditions when combined with tunnel drainage, the drawdown on shallow groundwater levels leads the vegetation to be vulnerable.

1. Introduction

Tunnel inflow during excavation and prolonged discharge by drainage during its life cycle out of the tunnel may cause groundwater resource depletion. Underground tunnel drainage alters the regional groundwater flow system and disturbs the local water balance (Gargini et al., 2008; Scheidler et al., 2017; Vincenzi et al., 2009). There is also evidence that highlights the adverse effects of deep underground drainage on the land surface (Butscher et al., 2011; Chiu and Chia, 2012; Kim et al., 2008; Kværner and Snilsberg, 2008; Li et al., 2016). As a result, potential impacts of tunnel drainage during underground excavations were evaluated from an environmental perspective (Huang et al., 2015; Li et al., 2018; Mossmark et al., 2017), and the impact on the hydrogeological environment (Yang et al., 2009) was considered. Recent studies have targeted the impact on terrestrial vegetation includ-

ing the groundwater drawdown (Li et al., 2018) and topsoil water dynamics (Gokdemir et al., 2020). Others have determined limiting tunnel drainage rate considering the ecological groundwater table level (Cheng et al., 2014, 2019). Although these works explained the relationship between discharge-induced drawdown and terrestrial vegetation, the contribution of atmospheric and climatic dynamics to the topsoil rooting zone during tunnel drainage was excluded.

The assessment results for the impact of tunnel drainage on terrestrial vegetation indicate that discharge-induced drawdown causes a reduction in plant growth (Zheng et al., 2017) and crop yield (Nesotto et al., 2009). Additionally, atmospheric studies emphasizing the interaction between terrain vegetation, soil water balance, and groundwater levels (Jiang et al., 2009; Leung et al., 2011; Martínez-De La Torre and Miguez-Macho, 2019; Rahman et al., 2015; Rihani et al., 2010) reveal the dynamics between subsurface and atmospheric conditions atmos.

* Corresponding author.

E-mail address: lixiaojun@tongji.edu.cn (X. Li).

Nomenclature	
AET	Actual evapotranspiration, mm d^{-1}
b	Shape-factor parameter for $R(\delta_r)$ (Eq. (A2)), dimensionless
ET	Evapotranspiration, cm d^{-1}
$H = H(z, t)$	Hydraulic head and water table level, m
$H_0 = H(z, t_1)$	Initial hydraulic head and water table level, m
$h = h(z, t)$	Soil water pressure, cm
h^*	Soil water pressure below which plants begin closing their stomata, cm
h_{\max}	Soil water pressure value below which roots extract water at the maximum rate until h^* , cm
h_{\min}	Allowable minimum soil water pressure at the soil surface, cm
h_w	Soil water pressure below which plants begin to wilt, cm
I	Canopy interception, mm
$K = K(h)$	Unsaturated hydraulic conductivity, m s^{-1}
K_{eff}	Effective hydraulic conductivity for layered soil profile, m s^{-1}
K_s	Saturated hydraulic conductivity, m s^{-1}
n	Exponent in the soil water retention function, dimensionless
P	Precipitation, mm
PET	Potential evapotranspiration, mm d^{-1}
$q_0 = q_0(t)$	Initial surface flux, cm d^{-1}
q_{\max}	Maximum constant surface flux, cm
q_p	Precipitation flux on the soil surface
q_R	Soil surface runoff flux
q_r^{root}	Possible root water extraction flux, cm d^{-1}
q_{r_0}	The potential transpiration flux, cm d^{-1}
q_r	Potential water extraction flux as function of vertical coordinate also referred to as the spatial distribution of q_{r_0} over the rooting zone, cm d^{-1}
q_{r_a}	Actual transpiration flux, cm d^{-1}
q_e	Potential evaporation flux, cm d^{-1}
q_{e_a}	Actual evaporation flux, cm d^{-1}
$R(\delta_r)$	Root length density distribution, cm $^{-3}$
$R(\delta_r)'$	Normalized water uptake distribution, unitless
R_{avg}	Medium root length density, cm $^{-3}$
RWU	Root water uptake, cm d^{-1}
S_s	Specific storage, m $^{-1}$
SPAC	Soil-Plant-Atmosphere Continuum
t	Time, d
t_0	Time when simulation begins, d
t_1	Initiation time of drawdown induced by tunnel drainage, d
t_2, t_3	Intermittent times that represent the duration after the tunnel drainage, d
t_4	The time water table stagnates, and drawdown stops, d
W	Net volumetric sink/source term, m $^3 m^{-3} s^{-1}$
z	Vertical coordinate, cm
$z_b = z_b(t)$	Water table level and lower boundary value, cm
z_{\max}	Depth of rock surface, cm
α	Empirical parameter in the soil retention function, d $^{-1}$
α_d	Value of α for drying condition of the soil water retention function, d $^{-1}$
α_w	Value of α for wetting condition of the soil water retention function, d $^{-1}$
β	Soil surface slope angle, degrees
δ	Rooting depth, cm
δ_e	Effective rooting depth which represents 50% of the total rooting depth, cm
δ_r	Relative root length normalized by δ , dimensionless
δ_r^{\max}	The maximum relative rooting depth, cm
δ_w	The portion of the rooting depth which corresponds to h_w , cm
$\theta = \theta(h)$	Soil water content, m $^3 m^{-3}$
θ_r	Residual soil water content, m $^3 m^{-3}$
θ_s	Saturated soil water content, m $^3 m^{-3}$
θ_s^d	Saturated soil water content of the drying condition, m $^3 m^{-3}$
θ_s^w	Saturated soil water content of the wetting condition, m $^3 m^{-3}$
$\mu(h)$	Root water uptake as a function of soil water pressure, dimensionless
ω	Modified Budyko model parameter; referred to as the shape parameter, dimensionless

Therefore, it is critical to include the association between topsoil water content and atmospheric forcing in the assessment of tunnel drainage.

In this study, “vulnerability” stands for the negative impact on vegetation due to the wilting of the terrestrial vegetation, that occurs when soil water pressure in the rooting zone reduces to the wilting point (Gokdemir et al., 2020), which is denoted as the point at which the plants cannot retrieve necessary water for their survival (Kirkham, 2014). If wilting point conditions persist, terrestrial plants start to die off, and vulnerability conditions are met. The occurrence of vulnerability is primarily related to infiltration and soil water storage. Thus, the increased water storage in the soil inhibits the occurrence of vulnerability. Therefore, the vulnerability is controlled by the amount of water in the soil. In ideal conditions, the resources of soil water storage are groundwater and rainfall for the topsoil; the assessment of vulnerability requires consideration of both sources.

This research considers the evaluation of environmental impact induced by deep tunnel drainage from the soil-plant-atmosphere continuum (SPAC) perspective (Norman and Anderson, 2004). In this context, the long-term aridity of the field is important based on atmospheric and climatic factors. Regions with a high rate of increased aridity are expected to be more vulnerable (Spinoni et al., 2015). However, in the case of shallow water table depths, plants may shift sufficient supplies of water needed for their survival against aridity (Cui and Shao, 2005). The water storage that remains inside the soil and accessible by vegetation is called plant-available water, supplied from groundwater as an essential source for vegetation survival, especially in prolonged dry seasons (Yang et al., 2017). Thus, empirically based estimates for water storage associated with hypothetical and real cases are proposed, including plant-available water in the soil (Milly, 1994; Yang et al., 2009; Yokoo et al., 2008). A semi-empirical approach is included in this study to evaluate the relationship between soil moisture dynamics and monthly variations in soil water storage in the vulnerability assessment. The primary form of the Budyko framework approach (Budyko, 1958, 1974) was considered, and represents the relationship between the ratio of actual evapotranspiration (AET) to precipitation (P) and aridity as the ratio of potential evapotranspiration (PET) to precipitation.

This study focuses on including the atmospheric and climatic components to the tunnel drainage impact by proposing an assessment method that can analyze the interactions between atmospheric and climatic conditions and groundwater table drawdown in soil media from a vulnerability perspective. Unlike previous attempts, this work provides an impact assessment, including the soil layer's water dynamics and the rooting zone coupling with atmospheric conditions. For this purpose, the vulnerability assessment method is employed on a specific case study to evaluate the vulnerability of terrain vegetation according to the difference in aridity. Accordingly, this study is organized as fol-

lows: **Section 2** introduces the methodology, including the sub-sections of vulnerability assessment method, and brief definition of groundwater seepage and transient topsoil model components. **Section 3** summarizes the study site, and, followed by a subsection that presents the design of hypothetical case study scenarios and atmospheric boundary conditions. **Section 4** summarizes the results of the application of vulnerability assessment method and soil water storage analysis from the Budyko perspective. The study is finalized with discussions in **Section 5**, and a summary and conclusion in **Section 6**.

2. Methodology

2.1. Vulnerability assessment

In this section, the relationship of the proposed vulnerability assessment framework with atmospheric forcing under the influence of tunnel drainage is introduced. The components that link SPAC perspective to vulnerability according to local climate are explained.

2.1.1. Assessment method based on atmospheric factors

The vulnerability assessment method is a product of the integration of numerical modeling with empirical concepts. In this context, the data flow of the method is designed to feed the topsoil and groundwater models. The vulnerability analysis was conducted using the outcomes of the topsoil model, where the effect of daily atmospheric conditions was analyzed using dynamic root-zone wilting. The changes in soil water storage were evaluated depending on the climatic difference on a yearly scale using Budyko-type analysis (Fig. 1d).

The vulnerability assessment method employs the following stages:

- Groundwater seepage model for water table distribution,
- Topsoil model based on a single column perspective for soil water pressure distributions,
- Dynamic root-zone wilting for the transient model,
- Budyko-type analysis for the soil water storage under longer term climatic changes,
- Summary based on the outcomes of vulnerability analysis.

The sequential nature of the vulnerability analysis gives the freedom to evaluate the system from hourly to yearly time scales. Hourly processes such as canopy interception and rainfall, daily process of evaporation, and monthly process of transpiration (Baird and Wilby, 1999; Savenije, 1997) can be included in the system individually. As the principal element of the method, the vulnerability assessment method provides a way to test the occurrence of vegetation wilting, and the exceedance of the plant-available water limits based on climatic conditions.

2.2. Groundwater seepage model

The groundwater seepage model provides the transient groundwater level distributions by using the finite-difference groundwater model MODFLOW (Harbaugh, 2005) to solve Eq. (1);

$$S_s \frac{\partial H}{\partial t} = -\nabla \cdot (-K_s \nabla H) + W \quad (1)$$

where S_s is the specific storage, H represents hydraulic head or water level, and K_s is saturated hydraulic conductivity that is assumed for homogeneous and isotropic porous media. W is the net volumetric sink/source term. The recharge process and tunnel drainage are considered as the source and the sink, respectively. Discretization is made based on the refined grid principle to represent the tunnel surface, where drainage nodes are located. On the tunnel surface, zero hydraulic head conditions are simulated ($\nabla^2 H = 0$) along the tunnel interior and seepage, and tunnel drainage flux is calculated.

In this research, we have focused on the representative drawdown conditions observed in the outcomes of the groundwater seepage

model after performing the tunnel drainage simulations. The validation was performed based on measured tunnel drainage flux and borehole groundwater hydraulic head measurements (Li et al., 2018).

2.3. Transient topsoil model

The topsoil model was prepared to solve unsaturated flow in the vadose zone. The Hydrus-1D model (Šimunek et al., 2013) is used to represent the components of SPAC as the topsoil model. Layered and homogeneous soil columns, rooting depth, water uptake model, and atmospheric boundary conditions were implemented into the model. Hydrus-1D was selected to employ a one-dimensional solution of the mixed form Richards equation as a verified tool that has been used in several prior studies on soil water dynamics and surface processes (e.g., Balugani et al., 2017; Šimunek et al., 2012; Soylu et al., 2011; Zlotnik et al., 2007).

The topsoil model is designed to respond to three components: one for the net infiltration on the ground surface (Eq. (2)), another for the root water uptake (RWU), and one for the deep or shallow soil groundwater table. The first component is considered as the mass balance on the soil surface:

$$q_0 = q_P \cos \beta + q_R - q_\epsilon \quad (2)$$

where q indicates water fluxes and q_0 stands for infiltration, with subscripts of surface runoff (R), daily precipitation (P), and evaporation (ϵ) that represent aggregate soil and canopy evaporation, and where β is the surface slope angle. In this study, the unit soil column approach is adopted (Dagan and Bresler, 1983; Rubin and Or, 1993) (See Fig. 2) and q_0 is imposed as the boundary condition at the ground surface. Infiltration without ponding is assumed on a flat soil surface ($\beta = 0$).

The potential root uptake q_τ at $z \leq \delta$ can be calculated from q_{τ_0} , which is included in the topsoil model as a function of relative rooting depth (δ_r).

$$q_\tau = q_{\tau_0} R(\delta_r)' \text{ for } z \leq \delta \quad (3)$$

where (δ_r) is the normalized soil depth with rooting depth (z/δ), q_{τ_0} is the potential transpiration flux, which is assigned based on the dominant vegetation type at the study site, and the normalized water uptake distribution is $R(\delta_r)'$ (See Appendix A for the assumptions of RWU and integration into the rooting zone).

Integration of Eq. (3) over rooting depth leads to the actual transpiration flux:

$$q_{\tau_a} = \int_0^{\delta_{\max}} q_\tau^{\text{root}} d\delta \quad (4)$$

AET is calculated as the sum of q_{τ_a} and actual evaporation flux (q_{ϵ_a}) for a particular time period. The numerical solution of Richards equation (Eq. (5)) was obtained for atmospheric BC as

$$\frac{\partial \theta(z)}{\partial t} = \frac{\partial}{\partial z} \left[K(h) \left(\frac{dh}{dz} + 1 \right) \right] - q_\tau^{\text{root}}(z) \quad (5)$$

Accordingly, Eq. (5) was subjected to the following conditions (Neuman et al., 1974) for the soil surface (upper BC):

$$\left| K(h) \left(\frac{dh}{dz} + 1 \right) \right| \leq |q_{\max}| \text{ at } z = 0 \\ h_{\min} < h(t) < 0 \text{ at } z = 0 \quad (6)$$

where h_{\min} is the allowable minimum pressure head at the soil surface and determined based on the equilibrium between water vapor and soil water content, and q_{\max} is equivalent to potential evaporation or infiltration rate under the imposed atmospheric conditions.

Thus, q_{ϵ_a} is estimated by simulating soil water pressure by the imposed BCs (Eq. (6)) on (5) unless runoff conditions are met; then Eq. (5) is solved imposing atmospheric and groundwater table BCs that interact with RWU in the root zone. The relationship between unsaturated hydraulic conductivity, $K(h)$, and volumetric water content, $\theta(z)$, is modeled using the assumptions of the Mualem–van Genuchten soil hydraulic

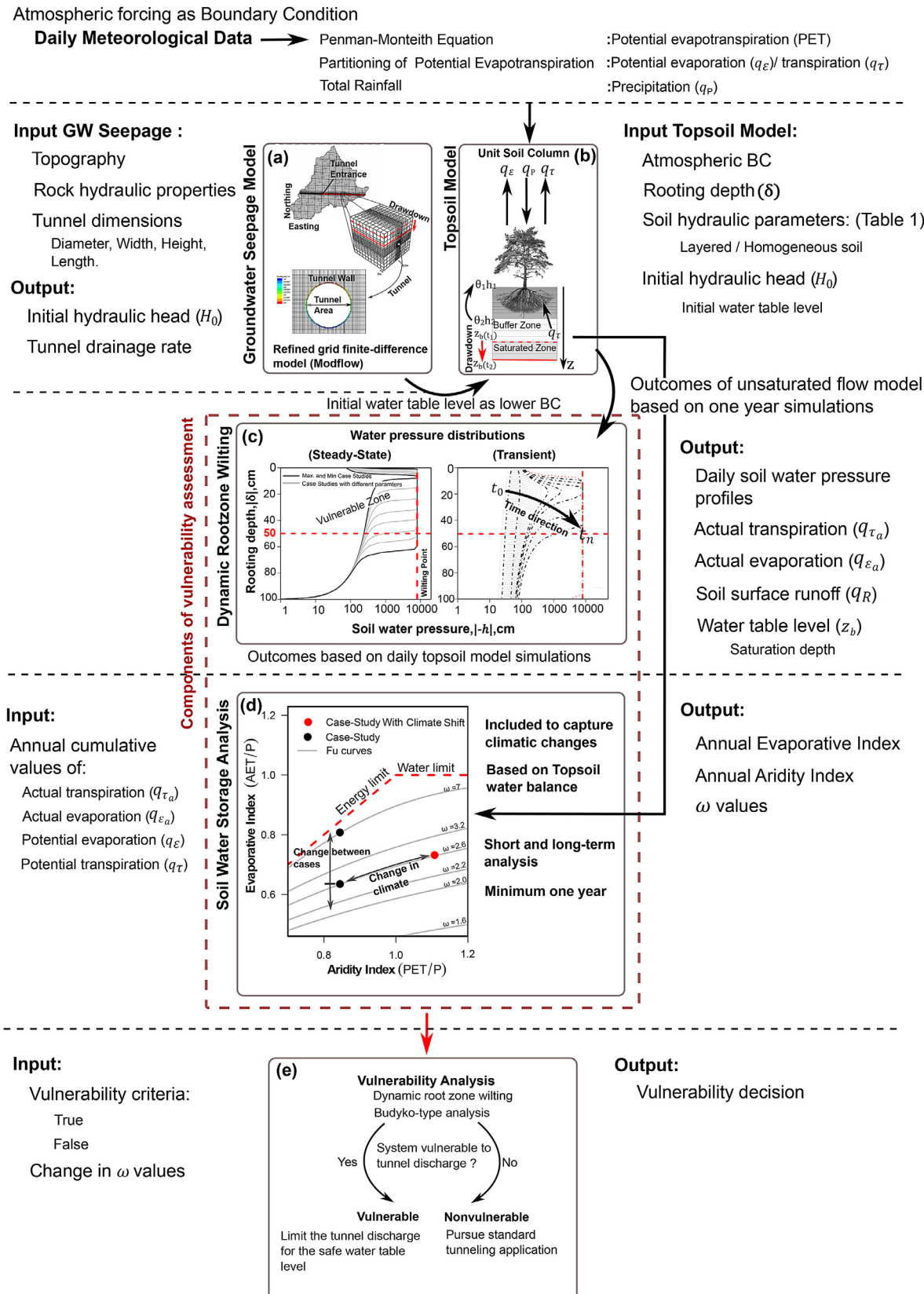


Fig. 1. Schematic outline of the suggested vulnerability assessment methodology with the case study application process from a SPAC perspective. The methodology contains five stages: (a) Groundwater seepage model for water table distribution, (b) Topsoil model based on single column perspective, vulnerability assessment analyses of (c) dynamic root-zone wilting for transient model, (d) A Budyko-type analysis for longer-term climatic changes, and (e) the summary and suggestions based on the outcomes of vulnerability analyses.

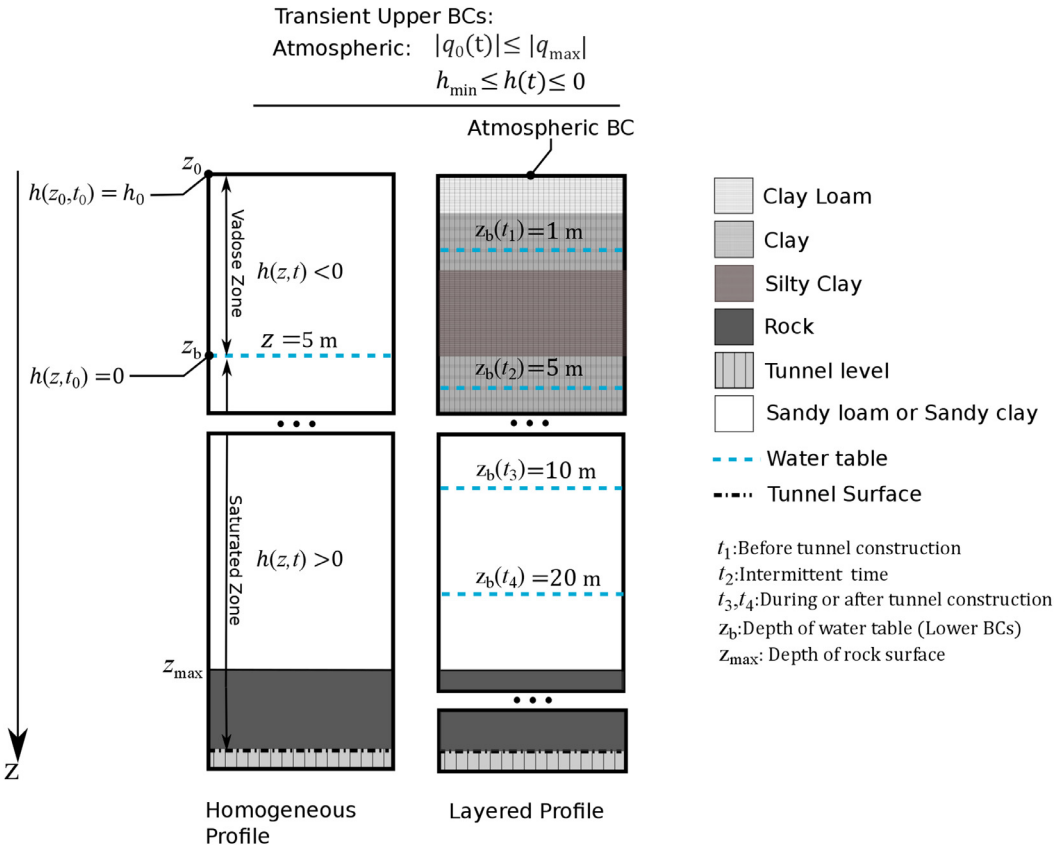


Fig. 2. Summary of 1D Unit soil profiles for selected cases of a layered soil with imposed upper and lower boundary conditions (BC). The profile represents a case with the same atmospheric upper BC, and with four water table (z_b) lower BCs before tunneling (t_1), intermittent time (t_2), after tunneling (t_3), and as the further time (t_4) for each condition. Previously specified root water uptake function and root length density distribution were also valid for all cases. Atmospheric BC is defined for layered and equivalent homogeneous profiles.

model under hysteretic conditions (For details see van Genuchten, 1980; Mualem, 1976).

As the third and final component, the groundwater table is designed as the lower boundary condition (z_b). Here, z_b represents a hydraulic head that can be changed due to the impact of tunnel drainage and received from the groundwater seepage model. z_b is equivalent to the initial hydraulic head (H_0) when the drainage conditions are non-existent. Four lower BCs are selected to represent a gradual reduction in water table levels for the same representative layered soil profile (Fig. 2). The bottom BCs are set to represent the scenario with different groundwater table, which is exposed to drawdown induced by tunnel drainage.

2.4. Dynamic root zone wilting

The method is created based on the dynamic root-zone wilting concept, which relies on a double vulnerability criterion on a single soil profile. These criteria represent two simultaneous conditions: (1) any condition that reduces topsoil water pressure to the wilting point (h_w), and (2) drying of 50% of the entire rooting depth (Gokdemir et al., 2020).

A combination of dynamic root-zone wilting and the empirically based method to estimate the water storage in soil column was implemented to extend the vulnerability of the case study. The soil profiles designed with an average rooting depth of 100 cm, where the root zone is assumed to be 70% of root water supply provided by the upper 50 cm as an effective rooting depth, δ_e (Bennett and Doss, 1960). $R(\delta_e)$ is distributed unevenly, such that δ_e represents approximately 80% of the root mass (Yu et al., 2007; Zhuang et al., 2001). The seasonal alterations in vegetation root density were neglected and R_{avg} was assumed

to be constant. Both criterion of vulnerability is met when the pressure of the entire δ_e reduced to h_w .

2.5. Soil water storage estimation

This study is designed to evaluate the effects of climatic conditions, combined with groundwater table drawdown as a representation of tunnel drainage effects, from a soil water storage perspective. For this, a Budyko-based framework was adopted, where climate effects were hypothetically evaluated using Fu curves (Fu, 1981; Zhang et al., 2004). A semi-empirical expression represents the water storage as follows:

$$\frac{AET}{P} = 1 + \frac{PET}{P} - \left(1 + \left(\frac{PET}{P} \right)^{\omega} \right)^{1/\omega} \quad (7)$$

where ω is the shape parameter, representing the long-term changes in soil water storage by drawdown and climate effect, for the Fu curves. These curves indicate the ensemble characteristics of soil properties, land cover, and vegetation class (Wang et al., 2016; Zhang et al., 2004).

A seasonal aridity index is defined as the ratio of potential evaporation to effective precipitation, where effective precipitation is the difference between rainfall and water storage change. Correspondingly, an evaporation ratio is defined as the ratio of evaporation to effective precipitation.

According to Eq. (7), ω is considered as a regulatory parameter that modifies the division of annual q_p between q_e and q_R (Zhang et al., 2004) and ranges between one and infinity. In the literature, typically, Budyko-type analyses were initially conducted using the original Budyko curve and with $\omega = 2.6$ as the reference value (Chen et al., 2013; Donohue et al., 2012; Greve et al., 2016; Wang et al., 2016). Although the aggregate physical meaning of ω is defined clearly, alternate values

have been proposed for the shape factor from different regions with diverse landscape characteristics (Gunkel and Lange, 2017). Therefore, in the present work, Budyko-type analysis is covered for a wide range of Fu curves and ω values.

3. Study site and case study

This section designed to present the description of selected study site (Section 3.1), and the hypothetical case study (Section 3.2) includes the drawdown and atmospheric scenarios based on the study site information.

3.1. Study site

The highway connection tunnel is located in Yuexi County, Anhui Province, mid-eastern China, with a maximum depth of 548 m below ground surface and 7548 km long towards east to west direction. The tunnel was constructed into a deep aquifer in moderately weathered granite and gneiss rock bodies. The study site is an afforested area with Chinese Fir (*Cunninghamia lanceolata*) and various understory species. Along with rock types, the soil parent material is composed of residual clay soil over fully weathered gneiss and contains silty clay layers within it. The forestry area of the study site ($\sim 180 \text{ km}^2$) has soft soil layers predominantly formed by silt, and silty clay profiles up to 20 m in thickness above the tunnel zone. The region has typical climatic features of central-eastern China with a sub-tropical humid climate. According to the 34-year (1980–2014) data form Houshan Station, the majority ($\sim 70\%$) of rainfall occurs between May and November with an average annual precipitation of 1147.8 mm. The driest year (1995) received 775.7 mm rainfall while the wettest year (1990) received 1660 mm annual precipitation. The annual rainfall (946.4 mm) corresponding to the year after the tunnel construction was considered for the vulnerability assessment. During this year, further climatic and atmospheric evaluations were conducted based on the data collected from Yuexi Station, which is similar to the study area in terms of elevation (Fig. 3c).

3.2. Case study

A vulnerability assessment was conducted for the case study based on several scenarios related to forest cover, weather conditions, and soil types from the tunneling site. The assumptions for parameters representing soil components of the case study were made based on the field observations from the study site and preliminary feasibility reports of the tunnel project. In this section, representation of the case study for the model assumptions and simulations is presented.

The wilting dynamics were tested from two perspectives for the case study: i) the combined effect of tunnel-induced water drawdown and daily variation of atmospheric conditions, and ii) the summary of climatic condition of Mingtang Tunnel as the humid and sub-humid dry climate for a year. The impacts of different soil textures are evaluated inherently in all scenarios.

3.2.1. Assumptions for soil hydraulic parameters and topsoil model design

The assumptions for the topsoil model components and defined BCs are summarized in Table 1. The hypothetical scenarios are designed to assess vulnerability for different hydraulic heads on the tunnel after different drawdown conditions.

3.2.2. Scenarios and assumptions for atmospheric and climatic forcing

Although dynamic root-zone wilting is related to the daily change of soil water pressure in the root zone, the Budyko-type analysis is applied for a one-year period because the water storage accuracy of the method reduces for shorter periods (Donohue et al., 2007). The annual evapotranspiration (ET) is evaluated as an aggregate value for the Budyko-type analysis. The components of ET are separated to examine their impact on water pressure distribution (Savenije, 2004).

Table 1
Summary of the model design and boundary conditions with atmospheric forcing. Hydraulic properties of soil profiles for the Mingtang Tunnel were tabulated according to the Mualem-van Genuchten soil hydraulic model.

Soil Type	Depth (cm)	Case study design parameters and boundary conditions		Node spacing	Simulation Length	$\delta(\text{cm})^a$	$R_{\text{avg}}(\text{cm}^{-3})^b$	Water table (m), $z_0(t)$
		Constant	Atmospheric forcing					
Topsoil (Hydrus 1-D)	Daily	pressure head representing water table	1-D vertical soil column	0.1 - 25 cm	365 days	40 - 340 (100)	0.1	1.00
		$\theta_s^w(\text{cm}^3 \text{ cm}^{-3})$	$\theta_s^d(\text{cm}^3 \text{ cm}^{-3})$	$\alpha_w(\text{cm}^{-1})^d$	$\alpha_d(\text{cm}^{-1})^d$	n	$K_s(\text{m s}^{-1})$	$K_{\text{eff}}(\text{m s}^{-1})$
Clay-Loam c	0 - 60	0.095	0.370	0.410	0.043	0.019	1.31	7.2311E-07
Clay c	60 - 160	0.068	0.340	0.380	0.018	0.008	1.09	5.556E-07
Silty-Clay c	160 - 340	0.070	0.324	0.360	0.011	0.005	1.09	5.556E-08
Clay c	340 - 1500	0.068	0.340	0.380	0.018	0.008	1.09	5.556E-07
Homogeneous Soil hydraulic parameters								
Sandy-Clay c	0 - 1500	0.040	0.420	0.471	0.026	0.012	2.00	4.167E-07
Sandy-Loam c	0 - 1500	0.065	0.369	0.410	0.168	0.075	1.89	1.228E-05

^a Based on *ex-situ* information temperate mixed coniferous and bamboo forests similar to Mingtang region.

^b From the previously published distribution parameters of de Jong van Lier (2006).

^c Class average values for van Genuchten model (1980) from Carsel and Parrish (1988).

^d Values calculated based on the hysteresis ratios of $\alpha_w/\alpha_d = 2.24$ and $\theta_s^w/\theta_s^d = 0.9$ from the experiments that were conducted by Likos et al. (2014).^{*} The limits are defined with constant values of h_w at -0.49 MPa (-5000 cm) and h_w at -79 MPa (-8000 cm) for each layer type.

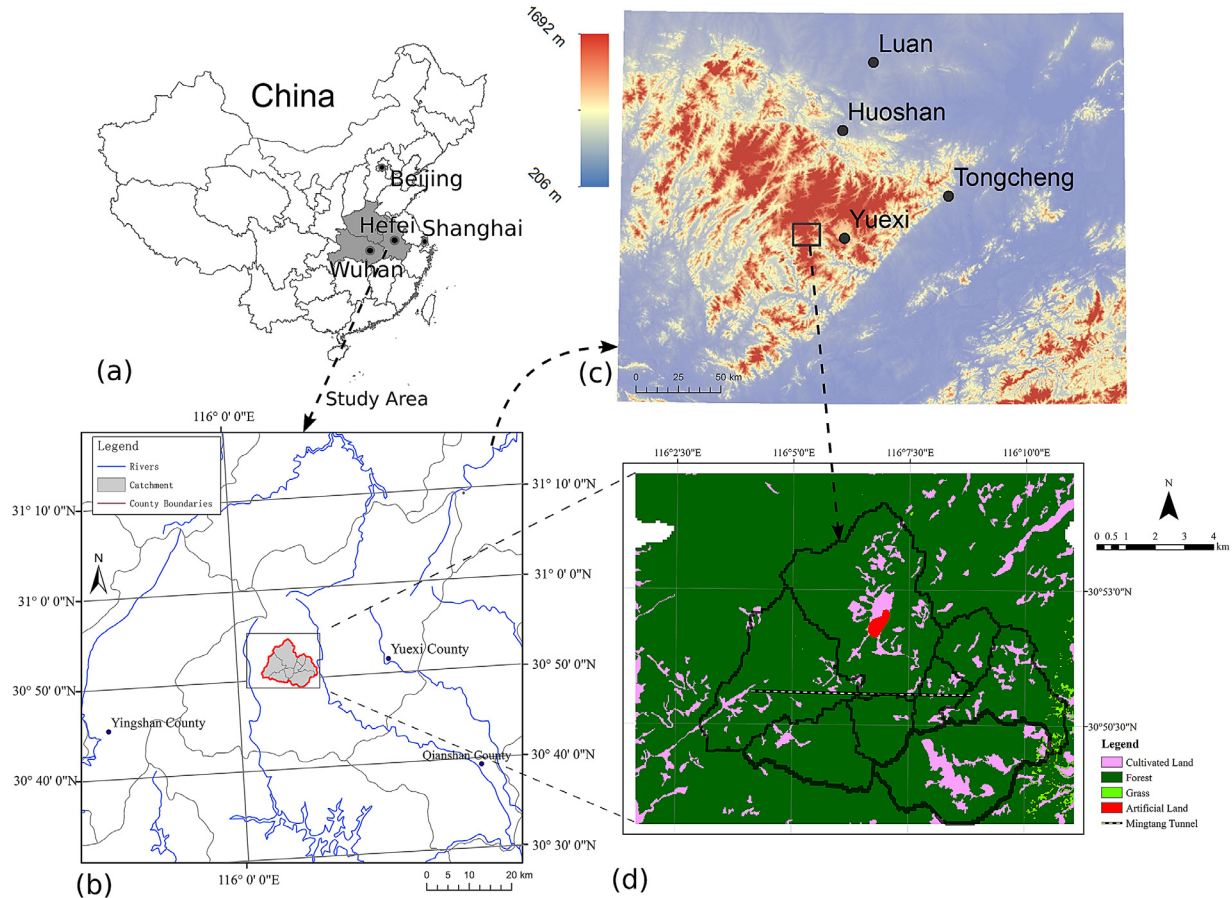


Fig. 3. Geographic information of the reference tunneling site: a) location of the tunnel site in eastern-central China; b) County borders and the tunnel catchment area with river networks and other water bodies; c) Locations of meteorological stations (gray points) in the Mingtang region with topographical feature map; d) Land characteristics of divided catchments corresponding tunnel construction from open-access global land cover data GlobeLand30 (Chen et al., 2017).

Total precipitation for the 2013–2014 tunneling year was 1135 mm, with a daily average of 13.8 mm/day, and a total annual calculated PET of 946 mm. According to UNEP, the 1997 classification for the Mingtang area is a typical humid climate (Aridity index: 0.83) (Grove, 1999).

Atmospheric BCs (Fig. 4) were converted from daily meteorological data corresponding to the tunnel construction year using the standardized Penman–Monteith method for tall canopies (Walter et al., 2001). A synthetic atmospheric condition was created based on the meteorological data under the assumption of reduced annual rainfall by 40% and the local surface air temperature elevation by 2 °C as the target future temperature in China (Fu et al., 2018) to create a more arid atmospheric condition. The altered synthetic atmospheric condition represents a sub-humid dry climate with reduced total precipitation of 464.7 mm, and a total annual PET of 680 mm (Aridity index: 1.46). Daily evaporative partitioning was assumed based on an empirical relationship between PET and q_r defined as $q_r = 0.73PET - 0.43$ in Ouyang et al. (2018). In the same work, a similar coniferous forest (dominated by *Cunninghamia lanceolata*) with approximately the same climatic conditions of Eastern China was considered. Plant parameters were selected based on maximal usage of soil water for coniferous forests.

A layered soil profile was assumed as a reference for the Mingtang area and compared with the homogeneous soil profiles. Atmospheric BCs were imposed on sandy-clay, sandy-loam, and layered soil profiles separately. The lower BCs were assigned for all profiles (Fig. 2) as the initial water table at t_1 was:

$$h(z, t_1) = 0 \text{ at } z = z_b = 1.0 \text{ m} \quad (8)$$

The second boundary at t_2 for intermittent drawdown condition was:

$$h(z, t_2) = 0 \text{ at } z = z_b = 5.0 \text{ m} \quad (9)$$

The lowest levels for the highest drainage impacts were:

$$\begin{aligned} h(z, t_3) &= 0 \text{ at } z = z_b = 10 \text{ m} \\ h(z, t_4) &= 0 \text{ at } z = z_b = 20 \text{ m} \end{aligned} \quad (10)$$

Lower BCs were arranged to simulate the impact of drainage on a shallower water table and on a relatively deep water table. Here, the shallow water tables ($z_b = 1.0\text{--}5.0\text{m}$) are where the saturated zone corresponds to the topsoil as the closest water level to the root zone. Model simulations were performed on a daily time scale for a year. An intra-annual analysis was conducted, and results reported for before (90th day), on (268th day), and after the peak rainfall (350th day), as marked by the vertical lines in Fig. 4.

4. Results

The results are organized according to the components of vulnerability assessment demonstrated in Fig. 1 and the scenarios summarized in Table 2. Sub-sections present the analysis of atmospheric (Section 4.1) and climatic (Section 4.2) effects on vulnerability.

4.1. Dynamic root-zone wilting under different water drawdown scenarios with atmospheric conditions

The analysis was conducted to explore the dynamics of vulnerability originating from, (i) transient pressure distributions for defined soil profiles, and (ii) various conditions of z_b representing before/after tunnel

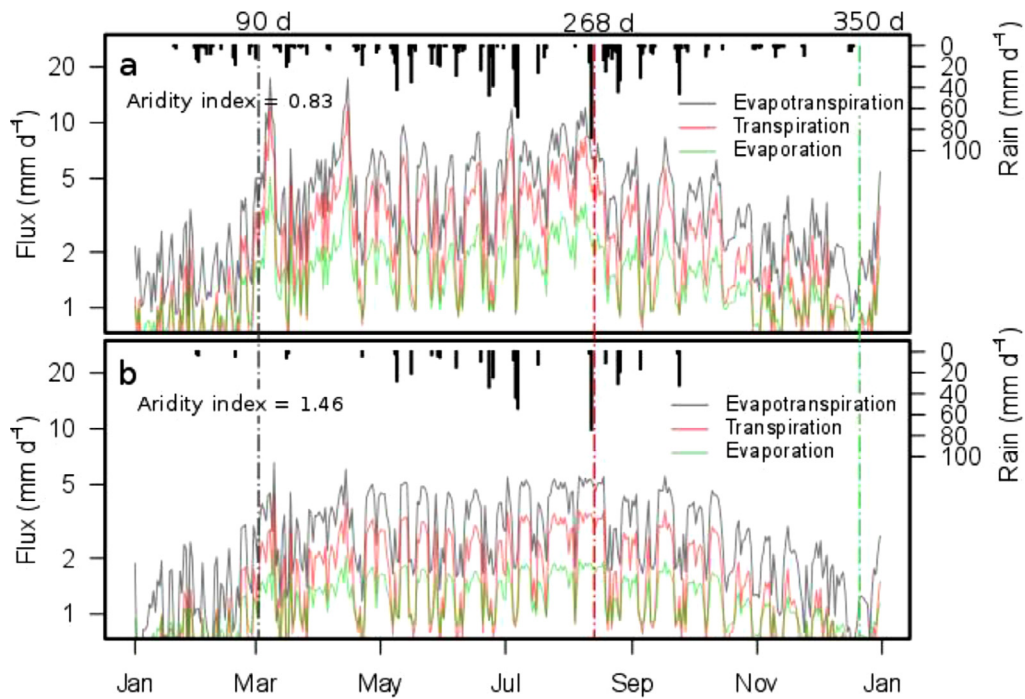


Fig. 4. The climatic representation of the Mingtang region based on the Houshan meteorological station with a) measured daily rainfall shown by black bars protruding from the top abscissa (right ordinate), and potential evapotranspiration (left ordinate). Designated days (90th, 268th, and 350th) were selected to represent episodic drying and wetting seasons for soil profile models and b) modified weather data to represent more arid conditions for the Mingtang region. Transpiration and evaporation values are also shown based on the assumed partitioning fraction.

Table 2

Matrix of topsoil simulation names classified based on soil column texture, water table levels, and imposed atmospheric conditions. Summary of scenarios are demonstrated with the associated topsoil simulations. Simulation names are decoded as climatic condition-soil type-water table.

		Climatic Scenarios							
		Humid Climate				Sub-Humid Dry Climate			
		Water table (m), $z_b(t)$							
Soil Scenarios	Soil Column	1	5	10	20	1	5	10	20
	Sandy-Loam	HLS1	HLS5	HLS10	HLS20	DLS1	DLS5	DLS10	DLS20
	Sandy-Clay	HSC1	HSC5	HSC10	HSC20	DSC1	DSC5	DSC10	DSC20
Soil Scenarios	Layered	HL1	HL5	HL10	HL20	DL1	DL5	DL10	DL20
		Water drawdown scenarios				Water drawdown scenarios			

drainage had occurred. The results of the two water drawdown scenarios from 5.0 m to 20 m (Fig. 5) as deep and shallow 1.0 m to 10 m (Fig. 6) are elaborated here. Intra-annual outcomes for atmospheric conditions were used corresponding to the tunnel construction year. Three selections were made for that year: the 90th and 350th day, representing the start and end days of the wet season, as the first and second dry periods in turn, and the 268th day as the day having the most abundant rainfall. The pressure profiles are shown for each selected day for the humid and sub-humid dry climate scenarios in Figs. 5 and 6. All intra-annual simulation outcomes based on changing groundwater levels are presented in Appendix B (Fig. B1).

Figs. 5 and 6 show the transient simulation results from the topsoil model for three contrasting days that differ in daily atmospheric conditions. Water pressure distributions for these three periods were grouped based on the three modeled soil profiles (homogeneous or layered) in a total of 24 simulation results according to three scenario groups (Table 2). Important physical observations were marked with numbers to facilitate understanding.

The intra-annual pressure distributions demonstrate that differences in z_b for deeper water table did not result in significant root-zone wilting, with the pressure curves representing simulations for the 20-m water table level mostly overlapping the ones for the 5-m water table level within the root zone (DL5-DL20). The same behavior was observed also for the sandy-clay soil scenario (DSC5-DSC20).

Conversely, the topsoil pressure distribution for the case studies of a shallow water table of $z_b = 1\text{ m}$ lead to wilting by the change of water table to 10 m, such that, for all soil profiles, the shallow water table condition remains far from wilting conditions (④ in Fig. 6); however, a drawdown to the water level of 10 m under sub-humid dry climate conditions exhibits a transformation toward wilting. The wilting zone manifests itself on simulations of DL5, DL10, and DL20 in the same fashion by exhibiting an expansion of the wilting zone to 10 cm rooting depth first and then reaches to δ_e at the end of second dry period (② in Fig. 5 and ⑤ in Fig. 6d). Similarly, the homogeneous sandy-clay scenario with a sub-humid dry climate shows expansion of the wilting zone over the whole δ_e in the second dry period (⑤ in Fig. 6b). All of the above case studies meet the vulnerability conditions independent of soil type.

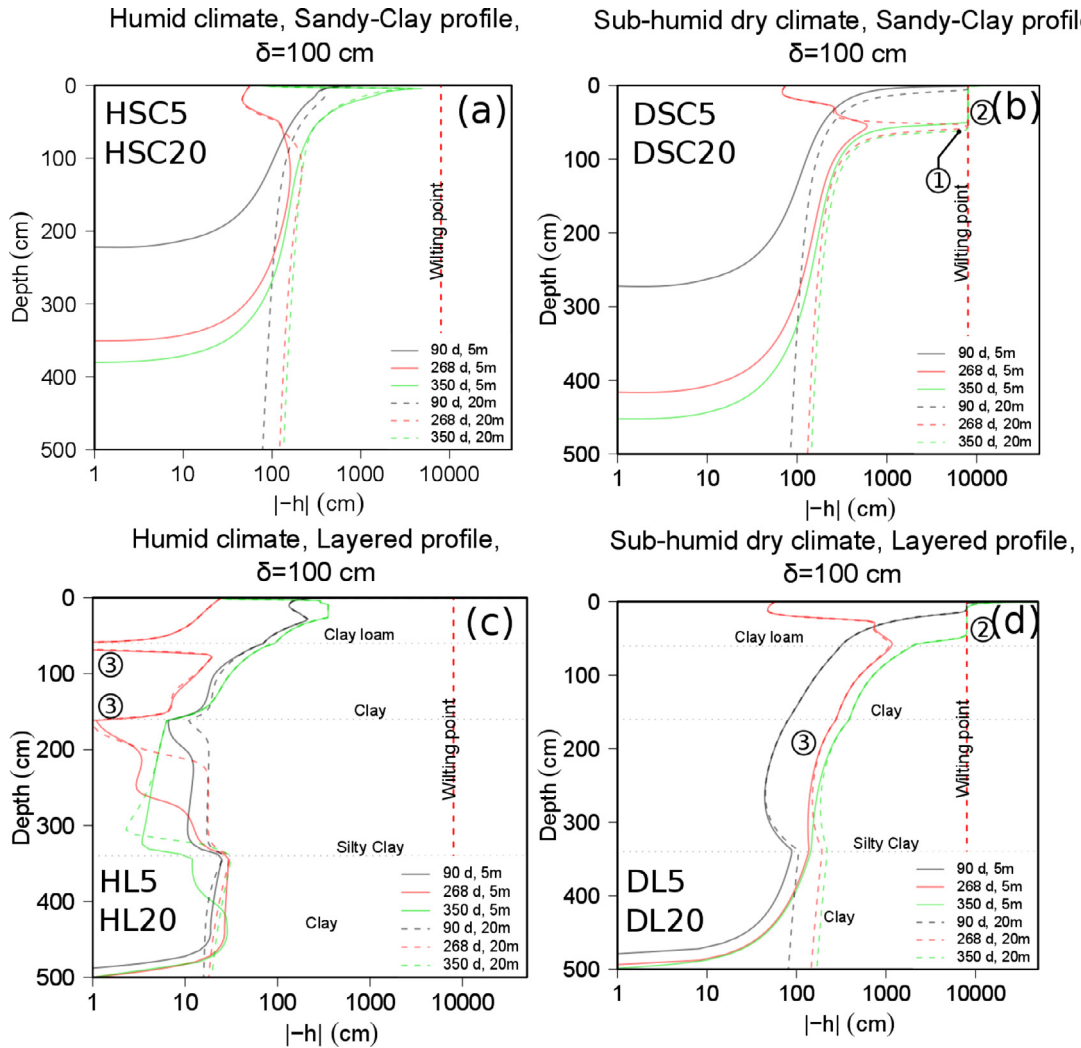


Fig. 5. A summary of the water table depths accompanying changes in water pressure distribution curves in the topsoil on three contrasting days considering the shallow water drawdown scenarios from 5 m to 20 m. Soil water pressure distributions are presented for a dry period (90th day, gray line), during a rainy period (268th day, red line), and the following dry period (350th day, green line) for a) humid, and b) sub-humid dry scenarios in a homogeneous sandy-clay soil profile, and c, d) layered soil profile. Circled numbers represent the numbered explanation provided in Section 4.2.

The intra-annual water pressure dynamics exhibited variability for the layered profile, based on soil heterogeneity. On the day of maximum rainfall, perched water accumulated at depths of 60 cm and 160 cm in the humid climate except for the shallow water with 1-m soil depth (HL5-HL20 in Fig. 5c ③, and HL10 in Fig. 6c). In contrast, a transient perched water table did not occur in the homogeneous case studies (Figs. 5a and 6a), and the soil remained saturated deeper than the maximum root depth throughout the year (2.0–4.0 m).

4.2. Soil water storage analysis for climatic scenarios

Although the previous analysis focused on the development of the wilting zone at a daily time scale, it did not reveal information from the aggregate change in soil water storage based on climatic scenarios. The Budyko-type analysis diagnoses the impact of shallow and deep groundwater level drawdown for yearlong water storage under humid and sub-humid dry climate conditions.

Fig. 7 summarizes the change in soil water storage at the end of the year, with each point representing the soil column with different settings. The components of the figure are summarized as follows:

- 1 Simulation results for each soil column (sandy-loam, sandy-clay, layered) are presented (salient points).

2 Experimental Fu curves (gray lines) and limit lines (dashed red line) are included to show the position of salient points relative to each curve.

The Budyko framework in Fig. 7 demonstrates two behaviors: i) the vertical movement of points (simulation outcomes) depends on their soil texture and changes in the water table, and ii) the horizontal movement of points because of an increase in aridity to a drier climate. The upward movement between and within the points indicates an evaporative increase equivalent to water loss, where the former represents a diversion from the layered soil profile (circle) and the latter the change in the shallow water table.

According to the Budyko framework, the evaporative index changes according to soil scenario. Fig. 7(①) shows an evaporative increase (water loss) toward the simulation of sandy-loam profiles larger than the sandy-clay profile relative to the layered profile. The evaporative increase for the sandy-loam (HLS1–5–10–20) is approximately 12% (136.2 mm) in humid and also 12% (55.8 mm) in sub-humid climates (DLS1–5–10–20) while, for the sandy-clay scenario it is approximately 2% (22.7 mm) for humid (HSC20) and 5% (23.24 mm) for sub-humid climates (DSC20). All of the simulation outcomes are scattered over a wide range of ω values from 3.3 to approximately 10.

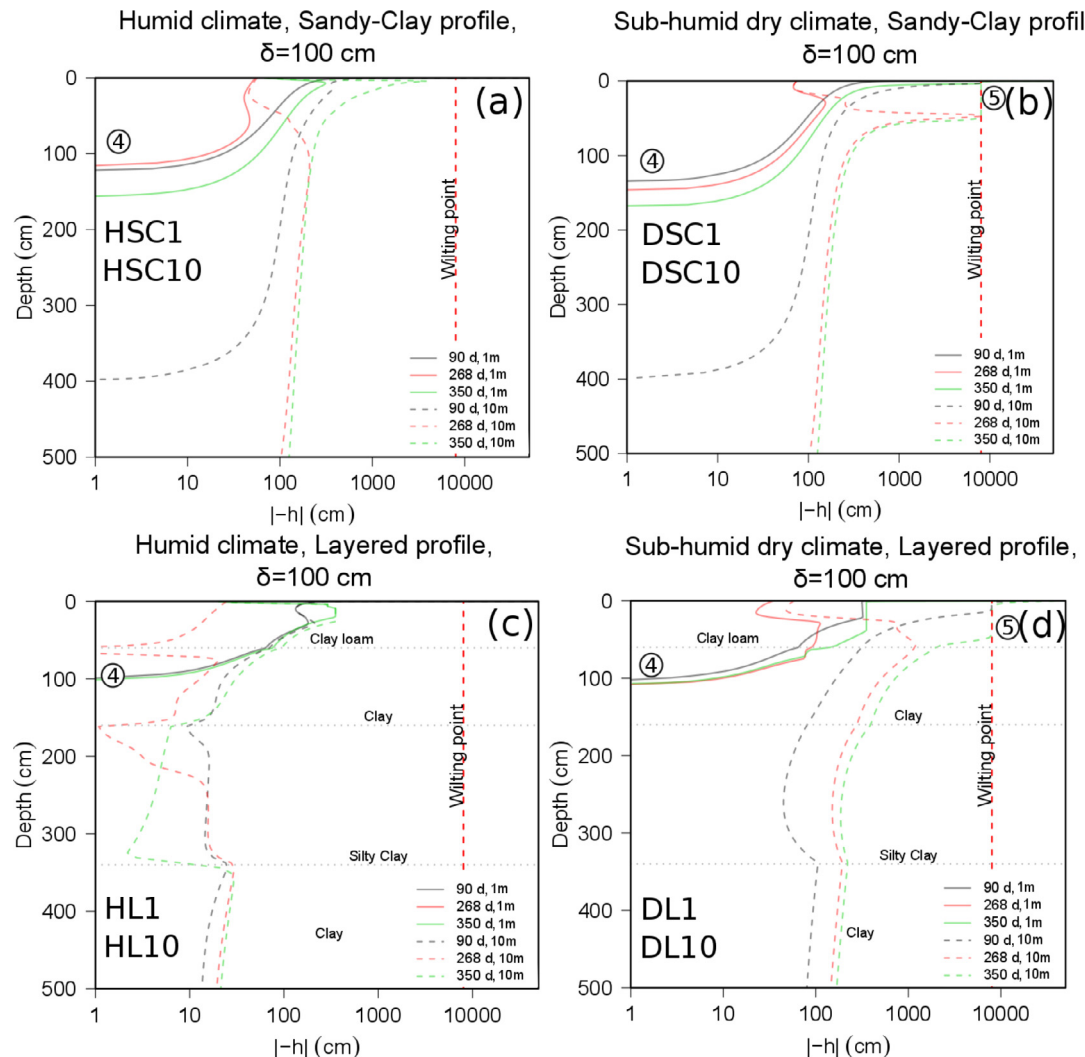


Fig. 6. Demonstration of topsoil water distributions and changes in rooting depth based on shallow water drawdown scenario from 1 m to 10 m water level depth. The demonstrated case studies for sandy clay profile are for (a) humid, and (b) sub-humid dry climate, and also for (c), (d) layered soil profiles.

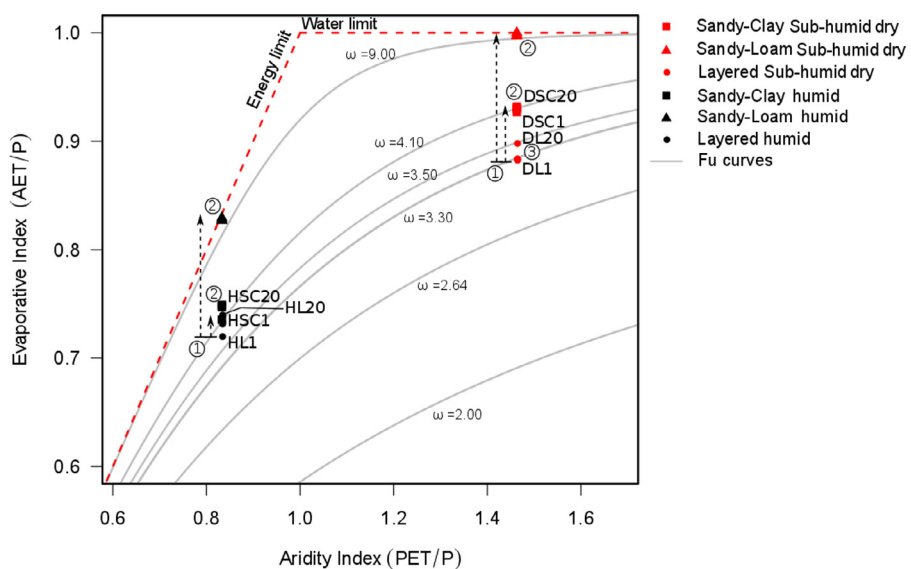


Fig. 7. Fu curves (continuous gray lines) on a Budyko plot for various shape parameter (ω) values, with standard energy and water limit curves (dashed red line). Points demonstrate the yearly balance with various simulations under the cover of a mature coniferous forest.

The response of the water levels, $z_b = 5$ m, 10 m, and 20 m to drawdown is not significant; the soil water storage does not change significantly for either sandy-clay or sandy-loam profiles (Fig. 7, ②). The sandy-loam scenario reached its limit for both climatic conditions, which indicates that all the available water was used for evapotranspiration. Conversely, the analysis shows that the variations in the water table are effective for water storage in the case of change from most shallow ($z_b = 1$ m) to deeper water level conditions (See simulations HL1-HL20, and DL1-DL20 in Fig. 7, ③).

5. Discussion

5.1. Vulnerability of shallow water table in soil under atmospheric conditions

In this study, the water levels were designated based on borehole readings of the study site, which, in reference to water levels, was deeper than 20 m until the rock bodies were exposed. There is evidence to suggest that saturated groundwater level fluctuates from 1 to 30 m depending on topography and seasonality (Fan and Miguez-Macho, 2010; De Graaf et al., 2015; Grogan and Galvão, 2006). This study follows the fact that the water table is the bottom limit of the vadose zone and regulates land drainage (Fan, 2015). Accordingly, drawdown scenarios were designed to represent the change in base level water tables (Kafri and Yechiel, 2010) induced by long-term tunnel drainage. The intra-annual outcomes of transient topsoil simulations suggest that humid atmospheric conditions do not lead to vulnerability even though pressure distribution in the root zone approaches the wilting point for sandy-loam profiles under drawdown to $z_b = 10$ m. Conversely, in sub-humid dry scenarios, plants cannot recover following a peak rainfall period after drawdown to deep water levels (DL20). Therefore, it can be inferred that atmospheric conditions are a distinctive factor for vulnerability in the case of deeper water level conditions.

The differences between soil water pressure distributions are not significant in the case of the drawdown scenario from 5 to 20 m (Fig. 5b and d). Conversely, the withdrawal of water table conditions from 1 to 10 m leads to a reduction in topsoil water pressure for both climatic conditions; topsoil pressure meets the vulnerability conditions when combined with sub-humid dry climate scenarios (Fig. 6b and d). The only scenario that does not show any influence by water drawdown is when layered soil is combined with humid climate (Fig. 6c). The top clay-loam layer with low conductivity carried the plant-available water yearlong despite the alterations to the saturated water level. Therefore, the textural variety caused the topsoil pressure behavior to remain non-vulnerable (Gokdemir et al., 2020; Yeh, 1989). However, when combined with a dry climatic scenario, low conductive layers cannot inhibit the decrease in the saturated level induced by drawdown (Fig. 6d), and simulations reach vulnerable conditions after peak rainfall (350th day).

5.2. Influence of climatic conditions on soil water storage under drawdown scenarios from a perspective of vulnerability

The profiles corresponded to Fu curves and associated ω (Eq. (7)) and demonstrated that the reference simulation results for the study site fit into a reasonable range of ω for humid basins in China (Wang et al., 2018) and the global values reported in Gunkel and Lange (2017). The changes in evaporation index due to the position of the reference condition in Fig. 7, revealed that a high permeability soil (sandy-loam) leads to a higher water loss. Specifically, the drainage capacity of the soil types impact aggregate soil water storage (Yokoo et al., 2008). Therefore, the sandy-loam simulations reached the limits for both climatic conditions (Fig. 7), indicating that all q_p infiltrated into the rooting zone was used. The sandy-loam profiles, thus, indicate a higher ω value (> 9). In humid climate conditions, the system may retrieve the water loss from the soil. However, the sandy-loam scenario in the sub-humid dry climate

leads to water stress conditions, wherein the plant-available water cannot be recovered. On the other hand, the soil profiles with less drainage capacity (layered, clay-loam) have lower evaporative index values despite their high potential of annual evapotranspiration (Salvucci and Entekhabi, 1995) compared to coarse-grained soil types (Eagleson, 1978; Istanbulluoglu et al., 2012). Within the simulations, textural differences dominated the change in water storage compared to the impact of variations in groundwater table.

From the impact of drawdown, the reference simulation outcomes are the most responsive to the withdrawal of shallow water levels. The general position of water storage outcomes prove that the drawdown scenario from shallow water ($z_b = 1$ m) is a condition where the system loses water (22.7 mm), and the drawdown seems insignificant in humid climates. However, from the perspective of vulnerability assessment, the results indicate that the same amount of water lost to groundwater (discharge via tunnel drainage) manifests itself through an increase of ω from 3.3 to 3.5 (Fig. 7, ③) and caused wilting of local vegetation under a sub-humid dry climatic condition (Fig. 6d). Even though the drawdown scenario from $z_b = 5$ m to 20 m indicates water loss, it does not represent a transition from non-vulnerable to vulnerable conditions (Fig. 5, HSC5-HSC20); hence a vertical shift in the Budyko framework was absent.

Overall, in a humid climate, the plant-available water remained existent throughout the year, and wilting conditions did not occur (Fig. 5c). Thus, the vegetation with a relatively lower water level would better resist the impacts of dry conditions when ample rainfall is available to create a perched water table (Robinson et al., 2005). Because the majority of the Mingtang region has layered soil, a deep drawdown, which exceeds vegetation root depth, would not cause the vegetation to wilt. However, the integrated vulnerability assessment method suggests that the study site region is sensitive to changes in climate. Therefore, a substantial increase in annual temperature or a decrease in annual rainfall may result in the development of vulnerable conditions for the same textural soil structure.

5.3. Vulnerability assessment method viewed from a behavioral perspective

In its basic form, the vulnerability assessment is based on the dynamic root-zone wilting and soil water storage analysis. From Section 3.1, the dynamic root-zone analysis evaluates the impacts on an hourly to daily basis; therefore, it is only possible to see the impact of climatic changes on an extended (decadal) time scale through the inclusion of a soil water budget. From a vulnerability perspective, the soil water budget analysis demonstrated two critical behaviors based on climatic and drawdown scenarios: (i) increase in aridity based on climatic alteration, and (ii) evaporative increase associated with the drawdown of groundwater level. For the specific case of this study, the former behavior led simulation results to follow specific Fu curves, which suggests essential insight but not a clear outcome in terms of vulnerability assessment, as it is not possible to know whether vulnerability conditions were satisfied. However, the latter behavior represents a minimal change in water storage compared to annual rainfall. While the dynamic wilting analysis captures the occurrence of vulnerability conditions, water budget (including Budyko-type) analysis reveals the amount of annual water loss to tunnel drainage that causes the vulnerability based on climatic scenarios.

Although the derived ω parameter values in the literature for basins and sub-basins exhibit a wide range of values, the cause of higher or lower Fu curves depends on the regional characteristics of the secondary controls (vegetation, land cover, topography, etc.) (Gunkel and Lange, 2017; Yang et al., 2009). Temporal (Zhang et al., 2008) and spatial (Xu et al., 2013) analysis scales of the investigation also control the curves independent of the prevalent climatic conditions. The analysis results in this study suggest that the values of ω parameters higher than the reference curve ($\omega = 2.6$) are linked to the most likely occurrence of vulnerability in the case of drained water storage.

6. Conclusion

The research presented in this study targets including atmospheric and climatic evaluation in the impact assessment of deep-tunnel drainage through integration to a vulnerability assessment method for terrestrial vegetation. The dynamics of vulnerability induced by drawdown were examined by integrating the dynamic root-zone wilting with soil water storage analysis from daily to annual scales, respectively. Accordingly;

- Intra-annual simulation results showed that the drawdown alone did not cause vulnerability in a humid climate after tunnel drainage. However, vulnerability conditions are met in a sub-humid climate.
- The shallower water conditions' response to drawdown exhibits behavior that the vegetation adapted to shallower water conditions were exposed to vulnerability after tunnel drainage.
- Combined with the intra-annual results, according to the approximate estimations derived from the soil water storage analysis, all sandy-loam soil simulation results demonstrated the highest evaporative potential.
- Discharge by tunnel drainage did lead to water loss in the representative scenarios for both climatic conditions. However, the case studies with high value in the Budyko framework satisfied the vulnerability conditions in the transient model through an increase in aridity.
- The analysis results support the idea that the change in climatic conditions is more deterministic than the groundwater level differences on shallow water from a vulnerability perspective.
- The interpretations of the outcomes of dynamic root-zone wilting and soil water storage analysis prove that the assessment is successfully links the impact of drainage induced drawdown and physical modeling.

Declaration of Competing Interest

The authors declare that they have no known competing financial interests or personal relationships that could have appeared to influence the work reported in this paper.

CRediT authorship contribution statement

Cagri Gokdemir: Conceptualization, Methodology, Software, Formal analysis, Investigation, Data curation, Visualization, Writing - original draft. **Yoram Rubin:** Supervision, Writing - review & editing. **Xiaojun Li:** Supervision, Resources, Writing - review & editing. **Hao Xu:** Investigation.

Acknowledgements

The research was conducted with support from the Natural Science Foundation of China (Grant No. 41877246), the Science and Technology

Plan Project of the Ministry of Transport of China (2013318J02120), the Tongji Civil Engineering Peak Discipline Plan, and the Fundamental Research Funds for Central Universities.

Supplementary materials

Supplementary material associated with this article can be found, in the online version, at doi:10.1016/j.advwatres.2020.103796.

Appendix A

This appendix contains the summary of assumptions for RWU in this research. The assumptions are linked to topsoil model defined in Section 3.2.

$R(\delta_r)'$ is normalized water uptake distribution that is given as

$$R(\delta_r)' = \frac{R(\delta_r)}{\int_0^{\delta_r^{\max}} R(\delta_r) d\delta_r} \quad (A1)$$

In Eq. (A1), $R(\delta_r)$ represents the root-specific length as the length of the root per unit volume soil. The denominator in the equation represents the normalization of the uptake distribution to ensure the integration of $R(\delta_r)$ to unity over the maximum relative rooting depth (δ_r^{\max}). The root zone is assumed as fully grown, and the uptake in the zone is controlled by $R(\delta_r)$ (dos Santos et al., 2017). Therefore:

$$R(\delta_r) = \frac{b^2 R_{avg}}{b + \exp^{-b} - 1} (1 - \delta_r) \exp^{-b\delta_r} \quad (b > 0). \quad (A2)$$

where R_{avg} is the average root density and b is a shape-factor parameter for the root distribution (Fig. A1b). Based on the design of root distribution, q_r can be linked to the soil water pressure depending on soil water availability (Feddes et al., 2001) as follows:

$$q_r^{\text{root}} = \mu(h) q_r \quad (A3)$$

where $\mu(h)$ is a dimensionless, stepwise water pressure response function, also called the plant limiting function. Fig. A1(a) illustrates the variation in the limiting function with h , which is a stepwise response function summarized in Eq. (A4) (Šimunek et al., 1992).

$$\mu(h) = \begin{cases} 0 & h \leq h_w \\ (h - h_w/h^* - h_w) & h_w < h < h^*, \\ 1 & h^* < h \end{cases} \quad (A4)$$

Here, the function represents RWU responses based on thresholds of wilting and stomatal closure (h^*) pressure values. From h^* up to maximum pressure point (h_{\max}) $q_r^{\text{root}}(z)$ is its maximum rate and diminishes after h^* to zero on h_w .

Appendix B

All intra-annual simulations results were demonstrated according to case studies in Fig. B1.

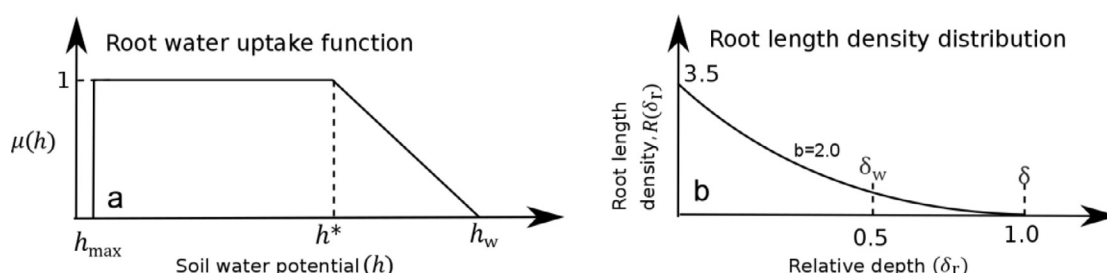


Fig. A1. (a) Root water uptake as a function of soil water pressure, modified from Feddes et al. (1978). h^* and h_w are the threshold pressure values according to the soil water deficit. h_{\max} is the maximum value for root uptake before the saturation ($h_{\max} < 0$). (b) Design of root length density distribution as a function of relative depth calculated by Eq. (A2) based on dos Santos et al. (2017), where δ_w indicates the threshold that satisfies vulnerability condition.

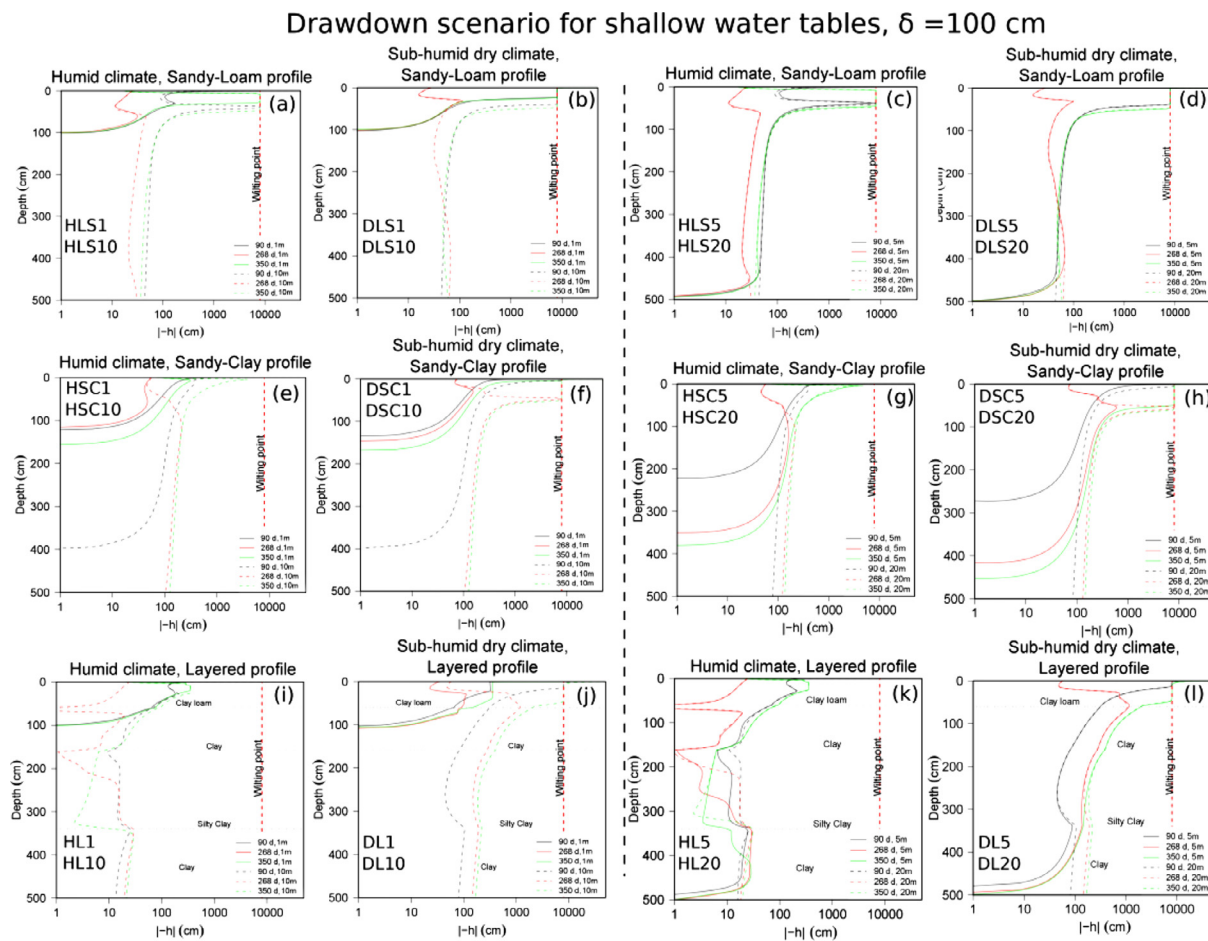


Fig. B1. Temporal inter-annual soil water pressure distributions for all case-studies divided based on shallow water and deep water table drawdown scenarios. Sandy-loam (a-d), clay-loam (e-h), and layered (i-l) profiles are presented where the left side columns represent humid climatic conditions while the right side represents sub-humid dry climatic conditions. Names of case studies are specified on corresponding pressure profiles.

References

- Baird, A.J., Wilby, R.L., 1999. Eco-hydrology: Plants and Water in Terrestrial and Aquatic Environments. Routledge Retrieved from <https://books.google.co.jp/books?id=MGRN5ULRUoC>.
- Balogun, E., Lubczynski, M.W., Reyes-Acosta, L., van der Tol, C., Francés, A.P., Metselaar, K., 2017. Groundwater and unsaturated zone evaporation and transpiration in a semi-arid open woodland. *J. Hydrol.* (Amst) 547, 54–66. <https://doi.org/10.1016/j.jhydrol.2017.01.042>.
- Bennett, O.L., Doss, B.D., 1960. Effect of soil moisture level on root distribution of cool-season forage species. *Agron. J.* 52, 204–207. <https://doi.org/10.2134/agronj1960.00021962005200040008x>.
- Budyko, M.I., 1958. The Heat Balance of the Earth's Surface. U.S. Department of Commerce, p. 259.
- Budyko, M.I., 1974. Climate and Life. Academic Press, New York.
- Butscher, C., Einstein, H.H., Huggenberger, P., 2011. Effects of tunneling on groundwater flow and swelling of clay-sulfate rocks. *Water Resour. Res.* 47 (11), 1–17. <https://doi.org/10.1029/2011WR011023>.
- Carsel, R.F., Parrish, R.S., 1988. Developing joint probability distributions of soil water retention characteristics. *Water Resour. Res.* 24 (5), 755–769. <https://doi.org/10.1029/WR024i005p00755>.
- Chen, J., Cao, X., Peng, S., & Ren, H. (2017). Analysis and applications of globeland30 : a review, 1–16. <https://doi.org/10.3390/ijgi6080230>.
- Chen, X., Alimohammadi, N., Wang, D., 2013. Modeling interannual variability of seasonal evaporation and storage change based on the extended Budyko framework. *Water Resour. Res.* 49 (9), 6067–6078. <https://doi.org/10.1002/wrcr.20493>.
- Cheng, Zhao, Li, Zou, Luo, et al., 2014. Limiting drainage criterion for groundwater of mountain tunnel.. *Journal of Central South University* 21 (12), 4660–4668. <https://doi.org/10.1007/s11771-014-2474-6>.
- Cheng, Zhao, Luo, Li, Li, Deng, Peng, et al., 2019. Analytical solution for the limiting drainage of a mountain tunnel based on area-well theory. *Tunnelling and Underground Space Technology* 84, 22–30. <https://doi.org/10.1016/j.tust.2018.10.014>.
- Chiu, Y.-C., Chia, Y., 2012. The impact of groundwater discharge to the Hsueh-Shan tunnel on the water resources in northern Taiwan. *Hydrogeol. J.* 20 (8), 1599–1611. <https://doi.org/10.1007/s10040-012-0895-6>.
- Cui, Y., Shao, J., 2005. The role of ground water in arid/semiarid ecosystems, Northwest China. *Groundwater* 43 (4), 471–477. <https://doi.org/10.1111/j.1745-6584.2005.0063.x>.
- Dagan, G., Bresler, E., 1983. Unsaturated flow in spatially variable fields: 1. Derivation of models of infiltration and redistribution. *Water Resour. Res.* 19 (2), 413–420. <https://doi.org/10.1029/WR019i002p00413>.
- Donohue, R.J., Roderick, M.L., McVicar, T.R., 2007. On the importance of including vegetation dynamics in Budyko's hydrological model. *Hydroclim. Earth Syst. Sci.* 11 (2), 983–995. <https://doi.org/10.5194/hess-11-983-2007>.
- Donohue, R.J., Roderick, M.L., McVicar, T.R., 2012. Roots, storms and soil pores: incorporating key ecohydrological processes into Budyko's hydrological model. *J. Hydrol.* (Amst) 436–437, 35–50. <https://doi.org/10.1016/j.jhydrol.2012.02.033>.
- Eagleson, P.S., 1978. Climate, soil, and vegetation: 6. Dynamics of the annual water balance. *Water Resour. Res.* 14 (5), 749–764. <https://doi.org/10.1029/WR014i005p00749>.
- Fan, Y., Miguez-Macho, G., 2010. Potential groundwater contribution to Amazon evapotranspiration. *Hydroclim. Earth Syst. Sci.* 14 (10), 2039–2056. <https://doi.org/10.5194/hess-14-2039-2010>.
- Fan, Ying, 2015. Groundwater in the Earth's critical zones: relevance to large-scale patterns and processes. *Water Resour. Res.* 3052–3069. <https://doi.org/10.1002/2015WR017037.Received>.
- Feddes, R.A., Hoff, H., Bruen, M.P., Dawson, T.E., de Rosnay, P., Dirmeyer, P., et al., 2001. Modeling root water uptake in hydrological and climate models. *Bull. Am. Meteorol. Soc.* 82 (12), 2797–2810. [https://doi.org/10.1175/1520-0477\(2001\)082<2797:MRWUIH>2.3.CO;2](https://doi.org/10.1175/1520-0477(2001)082<2797:MRWUIH>2.3.CO;2).
- Feddes, R.A., Kowalik, P.J., Zaradny, H., 1978. Simulation of Field Water Use and Crop Yield. Wiley Retrieved from <https://books.google.com/books?id=zEJzQgAACAAJ>.
- Fu, B.P., 1981. On the calculation of the evaporation from land surface. *Scientia Atmosphera Sinica* 5, 23–31. Retrieved from http://en.cnki.com.cn/Article_en/CJFDTOTAL-DQXK198101002.htm.
- Fu, Y.-H., Lu, R.-Y., Guo, D., 2018. Changes in surface air temperature over China under

- the 1.5 and 2.0 °C global warming targets. *Adv. Clim. Change Res.* 9 (2), 112–119. <https://doi.org/10.1016/j.accre.2017.12.001>.
- Gargini, A., Vincenzi, V., Piccinini, L., Zuppi, G.M., Canuti, P., 2008. Groundwater flow systems in turbidites of the Northern Apennines (Italy): natural discharge and high speed railway tunnel drainage. *Hydrogeol. J.* 16 (8), 1577–1599. <https://doi.org/10.1007/s10040-008-0352-8>.
- van Genuchten, M.T., 1980. A closed-form equation for predicting the hydraulic conductivity of unsaturated soils. *Soil Sci. Soc. Am. J.* 44 (5), 892. <https://doi.org/10.2136/sssaj1980.03615995004400050002x>.
- Gokdemir, C., Rubin, Y., Li, X., Li, Y., Xu, H., 2020. Vulnerability analysis method of vegetation due to groundwater table drawdown induced by tunnel drainage. *Adv. Water Resour.*, 103406. <https://doi.org/10.1016/j.advwatres.2019.103406>.
- De Graaf, I.E.M., Sutanudjaja, E.H., Van Beek, L.P.H., Bierkens, M.F.P., 2015. A high-resolution global-scale groundwater model. *Hydro. Earth Syst. Sci.* 19 (2), 823–837. <https://doi.org/10.5194/hess-19-823-2015>.
- Greve, P., Gudmundsson, L., Orlowsky, B., Seneviratne, S.I., 2016. A two-parameter Budyko function to represent conditions under which evapotranspiration exceeds precipitation. *Hydro. Earth Syst. Sci.* 20 (6), 2195–2205. <https://doi.org/10.5194/hess-20-2195-2016>.
- Grogan, J., Galvão, J., 2006. Physiographic and floristic gradients across topography in transitional seasonally dry evergreen forests of southeast Pará, Brazil. *Acta Amazonica. sciolo.* <https://doi.org/10.1590/S0044-59672006000400009>.
- Grove, A.T., 1999. World atlas of desertification. 2nd edition, edited by N.J. Middleton and D.S.G. Thomas, Arnold, London, 1997. No. of pages: x + 182. ISBN 0-340-69166-2. *Earth Surf. Process. Landforms* 24 (3), 280. [https://doi.org/10.1002/\(SICI\)1096-9837\(199903\)24:3<280::AID-ESP955>3.0.CO;2-7](https://doi.org/10.1002/(SICI)1096-9837(199903)24:3<280::AID-ESP955>3.0.CO;2-7).
- Gunkel, A., Lange, J., 2017. Water scarcity, data scarcity and the Budyko curve—an application in the lower Jordan river basin. *J. Hydrol.: Reg. Stud.* 12 (September 2016), 136–149. <https://doi.org/10.1016/j.ejrh.2017.04.004>.
- Harbaugh, A.W. (2005). MODFLOW-2005 : the U.S. Geological survey modular ground-water model—the ground-water flow process. Techniques and methods. <https://doi.org/10.3133/tm6A16>.
- Huang, Y., Bao, Y., Wang, Y., 2015. Analysis of geoenvironmental hazards in urban underground space development in Shanghai. *Natl. Hazards* 75 (3), 2067–2079. <https://doi.org/10.1007/s11069-014-1414-y>.
- Istanbulluoglu, E., Wang, T., Wright, O.M., Lenters, J.D., 2012. Interpretation of hydrologic trends from a water balance perspective: the role of groundwater storage in the Budyko hypothesis. *Water Resour. Res.* 48 (1), 1–22. <https://doi.org/10.1029/2010WR010100>.
- Jiang, X., Niu, G.-Y., Yang, Z.-L., 2009. Impacts of vegetation and groundwater dynamics on warm season precipitation over the Central United States. *J. Geophys. Res.: Atmos.* 114 (D6). <https://doi.org/10.1029/2008JD010756>.
- de Jong van Lier, Q., Metselaar, K., van Dam, J.C., 2006. Root water extraction and limiting soil hydraulic conditions estimated by numerical simulation. *Vadose Zone J.* 6 (3), 527. <https://doi.org/10.2136/vzj2007.0042L>.
- Kafri, U., Yechiali, Y., 2010. Groundwater Base Level Changes and Adjoining Hydrological Systems, 1st ed. Springer-Verlag, Berlin Heidelberg. <https://doi.org/10.1007/978-3-642-13944-4>.
- Kim, N.W., Chung, I.M., Won, Y.S., Arnold, J.G., 2008. Development and application of the integrated SWAT-MODFLOW model. *J. Hydrol. (Amst)* 356 (1–2), 1–16. <https://doi.org/10.1016/j.jhydrol.2008.02.024>.
- Kirkham, M.B., 2014. Field capacity, wilting point, available water, and the nonlimiting water range. *Princ. Soil Plant Water Relat.* 153–170. <https://doi.org/10.1016/B978-0-12-420022-7.00010-0>.
- Kværner, J., Snilsberg, P., 2008. The Romeriksporsten railway tunnel - drainage effects on peatlands in the lake Northern Puttjern area. *Eng. Geol.* 101 (3–4), 75–88. <https://doi.org/10.1016/j.enggeo.2008.04.002>.
- Leung, L.R., Huang, M., Qian, Y., Liang, X., 2011. Climate-soil-vegetation control on groundwater table dynamics and its feedbacks in a climate model. *Clim. Dyn.* 36 (1), 57–81. <https://doi.org/10.1007/s00382-010-0746-x>.
- Li, L., Tu, W., Shi, S., Chen, J., Zhang, Y., 2016. Mechanism of water inrush in tunnel construction in karst area. *Geomatics, Natl. Hazards Risk* 7 (sup1), 35–46. <https://doi.org/10.1080/19475705.2016.1181342>.
- Li, X., Li, Y., Chang, C.F., Tan, B., Chen, Z., Sege, J., et al., 2018. Stochastic, goal-oriented rapid impact modeling of uncertainty and environmental impacts in poorly-sampled sites using ex-situ priors. *Adv. Water Resour.* 111 (November), 174–191. <https://doi.org/10.1016/j.advwatres.2017.11.008>.
- Likos, W.J., Lu, N., Godt, J.W., 2014. Hysteresis and uncertainty in soil water-retention curve parameters. *J. Geotech. Geoenviron. Eng.* 140 (4), 04013050. [https://doi.org/10.1061/\(ASCE\)GT.1943-5606.0001071](https://doi.org/10.1061/(ASCE)GT.1943-5606.0001071).
- Martínez-De La Torre, A., Miguez-Macho, G., 2019. Groundwater influence on soil moisture memory and land-atmosphere fluxes in the Iberian Peninsula. *Hydro. Earth Syst. Sci.* 23 (12), 4909–4932. <https://doi.org/10.5194/hess-23-4909-2019>.
- Milly, P.C.D., 1994. Climate, soil water storage, and the average annual water balance. *Water Resour. Res.* 30 (7), 2143–2156. <https://doi.org/10.1029/94WR00586>.
- Mossman, F., Annertz, K.K., Ericsson, L.O., Norin, M., 2017. Hydrochemical impact of construction of the western section of the Hallandsås rail tunnel in Sweden. *Bull. Eng. Geol. Environ.* 76 (2), 751–769. <https://doi.org/10.1007/s10064-016-0962-7>.
- Mualem, Y., 1976. A new model for predicting the hydraulic conductivity of unsaturated porous media. *Water Resour. Res.* 12 (3), 513–522. <https://doi.org/10.1029/WR012i003p00513>.
- Neuman, S., Feddes, R.A., Bresler, E., 1974. Finite element analysis of two-dimensional flow in soils considering water uptake by roots: I. theory. *Soil Sci. Soc. Am. J.* 2 (39), 224–230.
- Norman, J.M., Anderson, M.C., 2004. Soil-plant-atmosphere continuum. In: Encyclopedia of Soils in the Environment, 4. Elsevier, pp. 513–521.
- Nosetto, M.D., Jobbág, E.G., Jackson, R.B., Szauder, G.A., 2009. Reciprocal influence of crops and shallow ground water in sandy landscapes of the Inland Pampas. *Field Crops Res.* 113 (2), 138–148. <https://doi.org/10.1016/j.fcr.2009.04.016>.
- Ouyang, S., Xiao, K., Zhao, Z., Xiang, W., Xu, C., Lei, P., et al., 2018. Stand transpiration estimates from recalibrated parameters for the Granier equation in a Chinese Fir (*Cunninghamia lanceolata*) plantation in Southern China. *Forests* 9 (4), 1–17. <https://doi.org/10.3390/f9040162>.
- Rahman, M., Sulis, M., Kollet, S.J., 2015. The subsurface–land surface–atmosphere connection under convective conditions. *Adv. Water Resour.* 83, 240–249. <https://doi.org/10.1016/j.advwatres.2015.06.003>.
- Rihani, J.F., Maxwell, R.M., Chow, F.K., 2010. Coupling groundwater and land surface processes: idealized simulations to identify effects of terrain and subsurface heterogeneity on land surface energy fluxes. *Water Resour. Res.* 46 (12), 1–14. <https://doi.org/10.1029/2010WR009111>.
- Robinson, B.A., Broxton, D.E., Viman, D.T., 2005. Observations and modeling of deep perched water beneath the pajarito plateau. *Vadose Zone J.* 4, 637–652. <https://doi.org/10.2136/vzj2004.0168>.
- Rubin, Y., Or, D., 1993. Stochastic modeling of unsaturated flow in heterogeneous soils with water uptake by plant roots: the parallel columns model. *Water Resour. Res.* 29 (3), 619–631. <https://doi.org/10.1029/92WR02292>.
- Salvucci, G.D., Entekhabi, D., 1995. Hillslope and climatic controls on hydrologic fluxes. *Water Resour. Res.* 31 (7), 1725–1739. <https://doi.org/10.1029/95WR00057>.
- dos Santos, M.A., De Jong Van Lier, Q., Van Dam, J.C., Bezerra, A.H.F., 2017. Benchmarking test of empirical root water uptake models. *Hydro. Earth Syst. Sci.* 21 (1), 473–493. <https://doi.org/10.5194/hess-21-473-2017>.
- Savenije, H.H.G., 1997. Determination of evaporation from a catchment water balance at a monthly time scale. *Hydro. Earth Syst. Sci. Discuss.* 1 (1), 93–100. <https://doi.org/10.5194/hess-1-93-1997>.
- Savenije, H.H.G., 2004. The importance of interception and why we should delete the term evapotranspiration from our vocabulary. *Hydro. Process* 18 (8), 1507–1511. <https://doi.org/10.1002/hyp.5563>.
- Scheidler, S., Huggenberger, P., Butscher, C., Dresmann, H., 2017. Tools to simulate changes in hydraulic flow systems in complex geologic settings affected by tunnel excavation. *Bull. Eng. Geol. Environ.* <https://doi.org/10.1007/s10064-017-1113-5>.
- Šimunek, J., Vogel, T., van Genuchten, M.T.(U.S.), S. L., 1992. SWMS-2D Code for Simulating Water Flow and Solute Transport in Two-dimensional Variably Saturated Media: Version 1.1. U.S. Salinity Laboratory Retrieved from <https://books.google.com/books?id=c-RyHQAAACAAJ>.
- Th. Šimunek, J., van Genuchten, M., Šejna, M., 2012. HYDRUS: model use, calibration, and validation. *Trans. ASABE* 55 (4), 1263. <https://doi.org/10.13031/2013.42239>.
- Šimunek, J., M. Šejna, A., Saito, H., Sakai, M., & Van Genuchten, M.T. (2013). The HYDRUS-1D software package for simulating the movement of water, heat, and multiple solutes in variably saturated media, Version 4.17, HYDRUS Software Series 3, (June), 343.
- Soylu, M.E., Istanbulluoglu, E., Lenters, J.D., Wang, T., 2011. Quantifying the impact of groundwater depth on evapotranspiration in a semi-arid grassland region. *Hydro. Earth Syst. Sci.* 15 (3), 787–806. <https://doi.org/10.5194/hess-15-787-2011>.
- Spinoni, J., Vogt, J., Naumann, G., Carrao, H., Barbosa, P., 2015. Towards identifying areas at climatological risk of desertification using the Köppen-Geiger classification and FAO aridity index. *Int. J. Climatol.* 35 (9), 2210–2222. <https://doi.org/10.1002/joc.4124>.
- Vincenzi, V., Gargini, A., Goldscheider, N., 2009. Using tracer tests and hydrological observations to evaluate effects of tunnel drainage on groundwater and surface waters in the Northern Apennines (Italy). *Hydrogeol. J.* 17 (1), 135–150. <https://doi.org/10.1007/s10040-008-0371-5>.
- Walter, I.A., Allen, R.G., Elliott, R., Jensen, M.E., Itenfisu, D., Mecham, B., et al., 2001. ASCE's standardized reference evapotranspiration equation. *Watershed Manage. Oper. Manage.* 2000 40499 (May), 1–11. [https://doi.org/10.1061/40499\(2000\)126](https://doi.org/10.1061/40499(2000)126).
- Wang, C., Wang, S., Fu, B., Zhang, L., 2016. Advances in hydrological modelling with the Budyko framework: a review. *Prog. Phys. Geogr.* 40 (3), 409–430. <https://doi.org/10.1177/0309133316620997>.
- Wang, T., Sun, F., Lim, W.H., Wang, H., Liu, W., Liu, C., 2018. The predictability of annual evapotranspiration and runoff in humid and nonhumid catchments over China: comparison and quantification. *J. Hydrometeorol.* 19 (3), 533–545. <https://doi.org/10.1175/JHM-D-17-0165.1>.
- Xu, X., Liu, W., Scanlon, B.R., Zhang, L., Pan, M., 2013. Local and global factors controlling water-energy balances within the Budyko framework. *Geophys. Res. Lett.* 40 (23), 6123–6129. <https://doi.org/10.1002/2013GL058324>.
- Yang, D., Shao, W., Yeh, P.J.-F., Yang, H., Kanae, S., Oki, T., 2009a. Impact of vegetation coverage on regional water balance in the nonhumid regions of China. *Water Resour. Res.* 45 (7). <https://doi.org/10.1029/2008WR006948>.
- Yang, F.-R., Lee, C.-H., Kung, W.-J., Yeh, H.-F., 2009b. The impact of tunneling construction on the hydrogeological environment of “Tseng-Wen reservoir Transbasin diversion project” in Taiwan. *Eng. Geol.* 103 (1), 39–58. <https://doi.org/10.1016/j.enggeo.2008.07.012>.
- Yang, F., Feng, Z., Wang, H., Dai, X., Fu, X., 2017. Deep soil water extraction helps to drought avoidance but shallow soil water uptake during dry season controls the interannual variation in tree growth in four subtropical plantations. *Agric. For. Meteorol.* 234–235, 106–114. <https://doi.org/10.1016/j.agrformet.2016.12.020>.
- Yeh, T.-C.J., 1989. One-dimensional steady state infiltration in heterogeneous soils. *Water Resour. Res.* 25 (10), 2149–2158. <https://doi.org/10.1029/WR025i010p02149>.
- Yokoo, Y., Sivapalan, M., Oki, T., 2008. Investigating the roles of climate seasonality and landscape characteristics on mean annual and monthly water balances. *J. Hydrol. (Amst)* 357 (3), 255–269. <https://doi.org/10.1016/j.jhydrol.2008.05.010>.

- Yu, G.R., Zhuang, J., Nakayama, K., Jin, Y., 2007. Root water uptake and profile soil water as affected by vertical root distribution. *Plant Ecol.* 189 (1), 15–30. <https://doi.org/10.1007/s11258-006-9163-y>.
- Zhang, L., Hickel, K., Dawes, W.R., Chiew, F.H.S., Western, A.W., Briggs, P.R., 2004. A rational function approach for estimating mean annual evapotranspiration. *Water Resour. Res.* 40 (2), 1–14. <https://doi.org/10.1029/2003WR002710>.
- Zhang, Lu, Potter, N., Hickel, K., Zhang, Y., Shao, Q., 2008. Water balance modeling over variable time scales based on the Budyko framework – model development and testing. *J. Hydrol. (Amst.)* 360 (1), 117–131. <https://doi.org/10.1016/j.jhydrol.2008.07.021>.
- Zheng, W., Wang, X., Tang, Y., Liu, H., Wang, M., Zhang, L., 2017. Use of tree rings as indicator for groundwater level drawdown caused by tunnel excavation in Zhongliang mountains, Chongqing, Southwest China. *Environ. Earth Sci.* 76 (15). <https://doi.org/10.1007/s12665-017-6859-3>.
- Zhuang, J., Yu, G.R., Nakayama, K., 2001. Scaling of root length density of maize in the field profile. *Plant Soil* 235 (1982), 135–142. <https://doi.org/10.1023/A:1011972019617>.
- Zlotnik, V.A., Wang, T., Nieber, J.L., Šimunek, J., 2007. Verification of numerical solutions of the Richards equation using a traveling wave solution. *Adv. Water Resour.* 30 (9), 1973–1980. <https://doi.org/10.1016/j.advwatres.2007.03.008>.